中國機械工程學刊第四十一卷第五期第 575~584 頁(民國一百零九年)
Journal of the Chinese Society of Mechanical Engineers, Vol.41, No.5, pp 575~584 (2020)

Dynamic Study of Pocket-Orifice Compensated Air Bearing System

Cheng-Chi Wang*, Chih-Wen Chang** and Tsui-Er Lee***

Keywords：Pocket-Orifice Compensated, Air bearing system, Chaotic motion.

ABSTRACT

Pocket-orifice compensated air bearing (PCAB) systems have been potential for use in high-rotational speed, and high-precision machine tool extensively and applied for a variety of mechanical engineering application. However, under certain operating conditions, PCAB systems exhibit non-periodic or chaotic motion as the result of a nonlinear pressure distribution within the gas film, gas supplied imbalances, an inappropriate design, and so forth. So, in order to understand and suppress as the bearing system occurs non-periodic motions and under what kind of operating conditions, the dynamic response of the PCAB system has been analyzed by using two different methods, namely a perturbation method and a hybrid numerical scheme combining the finite difference method and the differential transformation method. The key performances and solutions under different physical models obtained by these two methods are compared and verified. The dynamic behavior of rotor center has been examined under different operating conditions by bifurcation diagram, Poincaré maps, power spectra and Lyapunov exponents etc. The results reveals that the bearing number affects the orbits of the rotor which show chaotic behaviour in the interval of $16.41 \leqq \Lambda < 18.2$. The results obtained in this study can be used as a basis for future PCAB system design and the prevention of instability.

INTRODUCTION

PCABs have two major advantages including the air supply externally and pocket-orifice compensated design It also provides higher stiffness to increase the greater rotational stability. However, under specific operating conditions, PCAB systems exhibit non-periodic or chaotic motion as the result of a nonlinear pressure distribution within the gas film, gas supplied imbalances, an inappropriate design, and so forth. The mathematical theory of gas lubrication was first derived by Reynolds (1886) with partial differential equations related to pressure, density, relative motion and velocity. This equation is the famous Reynolds equation, and since then established the basis of fluid lubrication theory. In 1961, Malanoski et al. (1961) used capillary and orifice throttling to control the pressure distribution of hydrostatic bearings and improve the problem of insufficient oil film stiffness. This was the pioneer of passive throttles. However, Mayer et al. (1963) used a variable throttling device to bring better rigidity to the bearing system and achieved the same or even better results than other throttling methods such as membrane (1966). In 1970, Rowe et al. (1969) mainly invested considerable effort in the development of feedback throttles and also played a pivotal role. They were applied to thrust bearing systems in the form of thin film throttles and obtained relevant patent rights. Later, related scholars (1973) discussed the advantages and applications of this type of throttling method. Until 2000, Robert (2002) published an innovative active throttling device to improve the lack of thin film throttling in structure and overcome the shortcomings in manufacturing. And it can greatly improve the rigidity and bearing capacity of the system. It can be seen from the above-mentioned literature that the use of appropriate throttles in precision mechanical applications can indeed improve the performance of the bearing system, and active throttles had a better effect than passive ones.

Charki et al. (2013) provided a numerical simulation and an experimental study to assess stiffness and damping characteristics of thrust air bearings with multiple orifices. They applied finite element modeling to solve the non-linear Reynolds equation while taking into account the movement equation for the bearing. However, the above-mentioned documents still focus on oil film bearing systems instead of air film bearings, and they have not analyzed the vibration and dynamic

Paper Received September, 2020. Revised Sepfember, 2020, Accepted October, 2020, Author for Correspondence: Cheng-Chi Wang.

* *Professor, Graduate Institute of Precision Manufacturing, National Chin-Yi University of Technology, Taichung, Taiwan 41170, ROC.*

** *Assistant Professor, Department of Mechanical Engineering, National United University, Miaoli, Taiwan 36003, ROC.*

****Associate Professor, Office of Physical Education, Asia University, Taichung, Taiwan 41354, ROC.*

performance of the bearing rotors.

In the literature of rotor dynamic behavior, Bently (1974) found through experiments that the rotor oil film bearing system has 2nd and 3rd subharmonic vibrations. Child et al. (1982) used analytical methods to prove the existence of sub-harmonic vibration in the rotor bearing system. While the above documents are all aimed at oil film bearings, the rotor behavior of air film bearing systems is quite rare. Wang et al. (2017, 2018) solved the air film pressure and dynamic performance of a variety of air pressure bearing systems, and analyzed the rotor with trajectory diagrams, spectral analysis and bifurcation diagrams. The dynamic behavior of the shaft and journal centers and the flexibility effect of rotor were discussed. Their results found that the rotor and journal center have periodic, quasi-periodic or sub-harmonic motion under different operating conditions. It is also found that the system also caused chaotic motion (2019).

This paper focuses mainly on the analysis of the properties of PCAB systems and the range of dynamic behavior such a system exhibits under different operating conditions was also studied. In addition, the bifurcation properties of non-linear behavior produced by the system rotor are discussed, and are actually the means used to judge if the system displays chaos and to predict dynamic system trajectories accurately.

Design and Analysis of Pocket-Orifice Compensated Air Bearing System

The pocket-orifice compensated air bearing (PCAB) system is the integration of the hole-type air supply and the chamber (gas pocket) for secondary throttling. The special throttling method formed by the small hole throat (or ring) combined with the surface of the chamber is dynamic and static. The design of PCAB system is shown in Fig. 1. The main feature is that there are several (usually 4~8) shallow chambers evenly distributed along the circumferential direction on the bearing surface, and 1~2 air supply holes are set at a specific position in each chamber, and then small by external pressurized air orifice supply, through the small hole throat (or annulus) and the stepped surface of the shallow chamber, the hydrostatic effect of two throttling is produced. Due to the rotation of the rotor, the stepped surface of the chamber will produce a stepped dynamic pressure effect, which further strengthens the wedge dynamic pressure effect caused by the bearing eccentricity. Therefore, the cavity throttle air pressure bearing system is an ideal dynamic and static pressure mixed gas bearing system.

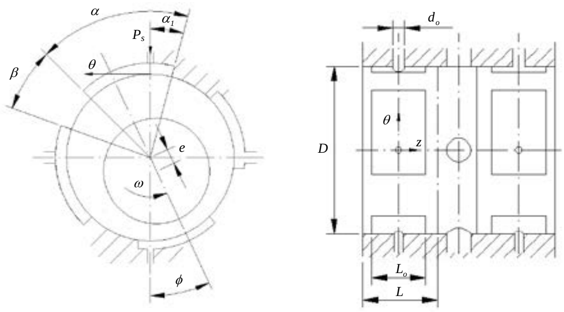

Fig. 1. Diagram of pocket-orifice compensated air bearing system.

At present, the difficulty faced by the industry is the problem of reduced life due to instantaneous contact friction, because the rotor is prone to collision during the start, stop or operation of the rotor, and if the bearing surface collides, the surface will be damaged and cause cyclones. The blockage prevents the gas from effectively exerting its supporting force, so unstable situations are more likely to occur, and the bearing and the rotor collide more frequently. The bearing system studied in this paper can overcome the above-mentioned problems, and has better stability and greater air film support.

The design of the orifice can be further divided into two types: small hole-shallow chamber throttle type and annular throttle type. These two bearings perform that the external pressure gas enters the bearing through the air supply holes distributed on the working surface of the bearing, and the throttling effect existed. It is related to the air supply hole and the difference is that the throttling properties of the two are different. The orifice throttling occurs at the smallest section of the orifice throat, and the throttling area is $\pi d_o^2/4$, which is a fixed throttling type. Annular throttling is produced on the cylindrical surface formed by the height of the clearance between the periphery of the small hole and the bearing. The throttling area is $\pi d_o h_o$, which is a variable throttling type. The detail of these two types are introduced as follows:

Small Hole-Shallow Chamber Throttle Air Bearing

The first type of PCAB is small hole-shallow chamber throttle air bearing and shown in Fig. 1. For the dynamic and static pressure of this bearing with shallow chambers, the pressure function must satisfy the dimensionless Reynolds Equation shown in Eq. (1), and the clearance function is calculated by Eqs. (2) and (3):

$$\frac{\partial}{\partial z}\left(\tilde{P}\tilde{h}^3\frac{\partial \tilde{P}}{\partial z}\right)+\frac{\partial}{\partial \theta}\left(\tilde{P}\tilde{h}^3\frac{\partial \tilde{P}}{\partial \theta}\right)=\Lambda\frac{\partial(\tilde{P}\tilde{h})}{\partial \theta}+\Lambda_s\frac{\partial(\tilde{P}\tilde{h})}{\partial \tau} \tag{1}$$

$$\tilde{h}=1-\varepsilon\cos\theta+j\delta \tag{2}$$

$$\delta = \begin{cases} 0, & as \ \ j = 1(out\ of\ chamber) \\ 1, & as \ \ j = 2(in\ chamber) \end{cases} \tag{3}$$

where ε is the eccentricity, $\tilde{h}$ is the gas film thickness, $\tilde{P}$ is the gas film pressure, μ is the viscosity coefficient, and θz is the coordinate system. If the bearing working area is D, its boundary is S

$$S = S_1 + S_2 \tag{4}$$

where S_1 is the outer boundary (atmospheric boundary), and S_2 is the inner boundary (intake boundary).

The boundary conditions are as follows:

$$S_1(z = L/D):\ \ \tilde{P} = 1 \tag{5}$$

$$S_2(z = 0):\ \ \frac{\partial \tilde{P}}{\partial z} = \frac{\Lambda_s P_s^2}{z \tilde{h}^3 \tilde{P}} \sqrt{\frac{1+\eta^2}{1+(\eta/\tilde{h})^2}}\ Q_1 \tag{6}$$

Where

$$Q_1 = C_D \begin{cases} \sqrt{\frac{2\kappa}{1+\kappa}\left(\frac{2}{1+\kappa}\right)^{\frac{1}{\kappa-1}}}, & as \ \ \frac{P_d}{P_s} \le \left(\frac{2}{1+\kappa}\right)^{\frac{1}{\kappa-1}} \\ \sqrt{\frac{2\kappa}{1+\kappa}}\left(\frac{P_d}{P_s}\right)^{\frac{1}{\kappa}} \sqrt{1-\left(\frac{P_d}{P_s}\right)^{\frac{\kappa-1}{\kappa}}}, & as \ \ \left(\frac{2}{1+\kappa}\right)^{\frac{1}{\kappa-1}} < \frac{P_d}{P_s} \le 1 \end{cases}$$

Annular Throttle Air Bearing

The second type mainly focuses on the analysis of double annular ring throttling air bearings. The double-ring air supply gap divides the bearing surface into three zones, A, B, and C, as shown in Fig. 2, namely zone A: ϕ1~ϕs1, zone B: ϕs1~ϕs2, C Area: ϕs2~ϕ2. Because the radius of the bowl is slightly larger than the radius of the sphere, the difference between them is the initial design clearance h_o of the bearing; the displacement of the ball in the axial direction (z) is e_z, if the upward displacement is positive, the gap gas film is convergent; if the downward formation is negative displacement, the interstitial air film is divergent.

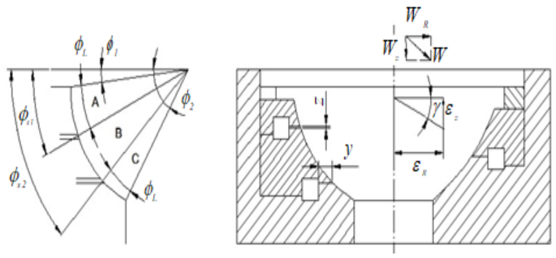

Fig. 2. Diagram of annular throttle air bearing.

The boundary condition of annular ring throttling air bearing is shown as Eq. (7)

$$\begin{cases} \tilde{P}(\varphi_1) = \tilde{P}(\varphi_1) = 1 \\ \tilde{P}(\varphi,\theta) = \tilde{P}(\varphi,\theta+2\pi) \\ \left.\frac{\partial \tilde{P}}{\partial \theta}\right|_{\theta} = \left.\frac{\partial \tilde{P}}{\partial \theta}\right|_{\theta+2\pi} \\ \left.\frac{\partial \tilde{P}}{\partial \varphi}\right|_{\varphi>\varphi_s} - \left.\frac{\partial \tilde{P}}{\partial \varphi}\right|_{\varphi<\varphi_s} = -\Lambda_s \frac{P_s^{\ 2}}{\tilde{P}2} Q_2 \left[\frac{csc\,\varphi}{H^3}\sqrt{\frac{1+\delta^2}{1+\left(\delta/_H\right)^2}}\right]_{\varphi_s} \end{cases} \tag{7}$$

Where Λ_s dimensionless bearing number; σ is dimensionless squeeze number; $\theta\ \phi$ are the coordinates in the circumferential and axial directions; μ is the gas viscosity coefficient; e_z is the axial eccentricity; e_R is the radial eccentricity; α is the meridian position angle of maximum air film thickness; C_r is the axial clearance; R_b is the radius of bearing (ball radius); ω_i is the angular velocity.

Through the steady-state numerical solution, the pressure distribution of the bearing in the areas A, B, and C can be obtained as follows:

For A area:

$$\tilde{P}_1 = \sqrt{\tilde{P}_a^{\ 2} + \frac{1+2\tilde{P}_a}{1+\alpha_1}\frac{F(\varphi)-F(\varphi_1)}{F(\varphi_{s1})-F(\varphi_1)}} - \tilde{P}_a \tag{8}$$

For B area:

$$\tilde{P}_2 = \sqrt{\tilde{P}_a^{\ 2} + \frac{1+2\tilde{P}_a}{1+\alpha_2}\frac{F(\varphi)-F(\varphi_{s1})}{F(\varphi_{s2})-F(\varphi_{s1})}} - \tilde{P}_a \tag{9}$$

For C area:

$$\tilde{P}_3 = \sqrt{\tilde{P}_a^{\ 2} + \left(1+2\tilde{P}_a\right)\left\{\frac{1}{1+\alpha_1} + \left[\frac{1}{1+\alpha_2} - \frac{1}{1+\alpha_1}\right]\left[\frac{F(\varphi)-F(\varphi_{s2})}{F(\varphi_2)-F(\varphi_{s2})}\right]\right\}} - \tilde{P}_a \tag{10}$$

Where $F(\varphi) = \int_0^{\varphi} \frac{d\psi}{cos\,\psi(1-\varepsilon\, sin\,\psi)^3}$, $\tilde{P} = \frac{P-P_a}{P_s-P_a}$, $\tilde{P}_a = \frac{P_a}{P_s-P_a}$, $\alpha_1 = \alpha_0^{\ *}\frac{\xi_1}{F(\varphi_{s1})-F(\varphi_1)}$, $\alpha_2 = \alpha_0^{\ *}\frac{\xi_2}{F(\varphi_2)-F(\varphi_{s2})}$, $\tilde{P}_i = \frac{P_i-P_a}{P_s-P_a}$ (i=1,2,3), $\alpha_0^{\ *} = \alpha_1^{\ *}\cos\varphi_{s1} = \alpha_2^{\ *}\cos\varphi_{s2}$, $\alpha_1^{\ *} = \frac{2\pi y h_o^3}{N_1 a_1 z^3}$, $\alpha_2^{\ *} = \frac{2\pi y h_o^3}{N_2 a_2 z^3}$.

The above Eq. (1) and the corresponding boundary conditions can be determined the relevant performance parameters of the small hole-shallow chamber bearing and annular throttling air bearing system during operation, including pressure distribution, bearing capacity, air film stiffness and damping coefficient. This paper also monitors and analyzes the dynamic behavior of the rotor, including dynamic trajectory, spectrum response, bifurcation behavior, Poincaré map, and Lyapunov exponents, which can further analyze under which operating parameters the system will cause instability for obtaining a stable PCAB system.

Results and Discussion of Numerical Simulation

This paper uses two different numerical methods to solve the PCAB system. The results show that the hybrid method by Wang et. al. (2017) combining the differential transformation method (DTM) and the finite difference method (FDM) has good agreement with the traditional perturbation method, and the results obtained by the perturbation method caused the instability phenomenon under some conditions and also showed that the hybrid method (DTM&FDM) has better accuracy than perturbation method for PCAB system. The comparison of the trajectory of the rotor center (X2, Y2) is shown in Table 1.

Table 1. Comparison of various numerical calculation results for rotor center displacement (For small hole-shallow chamber throttle bearing)

Methods	Operation condition /(X2,Y2)		$\Delta\tau$ 0.001	$\Delta\tau$ 0.01
Perturbation	m_r =3.2 kg Λ=4.5	X2	-0.1710583521	-0.1716278329
		Y2	0.1674424205	0.1673665742
Hybrid		X2	-0.1710556262	-0.1710558301
		Y2	0.1674877970	0.1674876574
Perturbation	m_r =4.85 kg Λ=4.5	X2	-0.2046182573	-0.2043519594
		Y2	0.2697106185	0.2698716188
Hybrid		X2	-0.2048917501	-0.2048919604
		Y2	0.2691034071	0.2691039593
Perturbation	m_r =2.61 kg Λ=9.38	X2	0.1121572809	0.1139494365
		Y2	-0.1086283727	-0.1088915074
Hybrid		X2	0.1128407276	0.1128409513
		Y2	-0.1086521957	-0.1086526408

For the stability of numerical analysis by hybrid method, the influence of different time intervals on the numerical value is completed, and the rotor center displacements of Poincaré cross section under different $\Delta\tau$ are compared. The numerical values are shown in Table 2.

Table 2. Numerical comparison of the Poincaré section of the rotor center at different time intervals τ (calculated by hybrid method; m_r = 3.47 kg, Λ = 3.8)

$\Delta\tau$	X 2(n T)	Y 2(n T)
π/300	0.0401841682	0.3643430301
π/400	0.0401867451	0.3643436712
π/500	0.0401884132	0.3643409123
π/600	0.0401848794	0.3643432969

It can be seen from the above numerical results that the hybrid method studied in this paper has good convergence and applicability for PCAB system, and the change in the rotor mass or the increase of bearing number can effectively be calculated for the trajectory of the system. At the same time, in order to shorten the time of subsequent calculation of the bifurcation characteristics of the system, the selection of the time interval is shown by the test results in Table 2 to obtain sufficient precision numerical results without being too samll. Therefore, in the subsequent dynamic analysis part, π/300 is used as the time interval calculation.

Dynamic behavior analysis - rotor mass as a bifurcation parameter

Take the small hole-shallow chamber throttle air bearing as an example, because the rotor mass and the bearing cause air flotation effect, and the rotor mass influences the strength of the air flotation effect, and then affect the stability of the overall system. Therefore, this section mainly analyzes the influence of the rotor mass on the gas bearing system. The bearing number is assumed as Λ=3.8, and the rotor mass is used as the bifurcation parameter:

From Fig. 3.1(a), 3.2(a),..., 3.8(a), it can be seen that the center of rotor (X2, Y2) behaves periodic situation (m_r=3.2 kg), and the trajectory is in a regular pattern. When the mass increases to 4.54 kg, the non-periodic phenomenon replaces the regular motion, and when the mass further increases to 4.85 kg, the periodic phenomenon is again appear. However, this stable phenomenon did not last long. When the rotor mass began to increase to 4.91 kg, the unstable behavior reappeared. It can be seen that the rotor mass is controlled below 3.2kg and the system can be relatively stable. As the rotor mass reaches 5.43, 5.48, 5.85, 5.93, the system all presents a non-periodic phenomenon.

Figure 3.1(b), 3.2(b),..., 3.8(b) shows the spectral response of the rotor center in the horizontal direction. Research shows that when the rotor mass is 3.2kg, The center of rotor presents a single-period movement, and when m_r=4.54kg, the spectrum response diagram (Figure 3.2(b)) shows that the rotor changes into a non-periodic state in the horizontal directions. When the rotor mass is increased to 4.85kg, the system reveals T-periodic motion; when the mass is changed to 4.91 and 5.48kg, the system switches to aperiodic motion. In addition, when the rotor mass is increased to 5.43, 5.85, 5.93kg, the system state shows sub-harmonic motion.

As shown in Fig. 4, the rotor mass is used as an analysis parameter to discuss the influence of different rotor masses on the system, and the mass range is set to be between 0.1 and 6.0 kg for actual operating conditions. It can be seen from Fig. 4(a) and (b) that when m_r <4.54 kg, the rotor center of the system exhibits T periodic motion in both the horizontal and vertical directions. This phenomenon can be proved by the Poincaré map shown in Fig. 5(a). However, when the mass increases to 4.54kg, this T periodic motion of the rotor is replaced by chaotic motion, and the chaos state can be formed by multiple discrete points shown in Fig. 5(b). The aperiodic motion proved that the system state is maintained within the range of $4.54 \leqq m_r < 4.85$kg. As the mass continues to increase to 4.85kg, the system will switch back to T-periodic motion (as shown in Figure 5(c)), and this motion is maintained within the range of $4.85 \leqq m_r < 4.91$kg. As the mass continues to increase to 4.91kg, the T-periodic of the PCAB system diverges into chaotic motion (as shown in Figure 5(d)). This type of motion is distributed in $4.91 \leqq m_r < 5.43$kg. This behavior is again converted to a subharmonic motion when the mass increases to 5.43kg, as shown in Fig. 5(e), this motion is distributed in $5.43 \leqq m_r < 5.48$kg. When the rotor increased to 5.48kg, chaotic motion appeared again, as shown in Fig. 5(f), this motion was distributed in $5.48 \leqq m_r < 5.85$kg.

Then, if the rotor mass continues to increase to 5.85kg, the non-periodic trajectory of the system turns into a subharmonic motion. As shown in Figs. 5(g) and 5(h), the cross-sectional view produces multiple irregular discrete points. This type of movement is distributed at 5.85~6.0kg.

For the chaotic behavior part, the maximum Lyapunov exponents are used for interpretation and further verification in the implementation of this study. From Figs. 6(a)-6(h), we can see that when m_r = 3.2, 4.54, 4.85, 4.91 , 5.43, 5.48, 5.85, 5.93 kg, the maximum Lyapunov exponent tends to zero or less than zero, the system is non-chaotic behavior. When m_r = 4.54, 4.91, 5.48kg, as shown in Figures 6(b), 6(d), and 6(f), the index is greater than zero, so the motion state of the system is indeed chaotic, which is consistent with the above results .

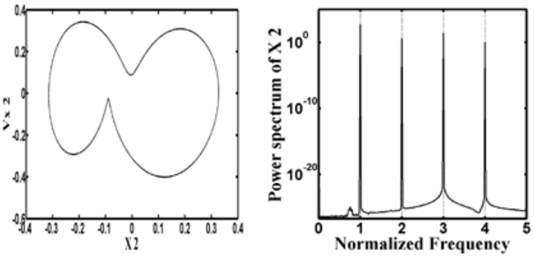

3.1(a) 3.1(b)

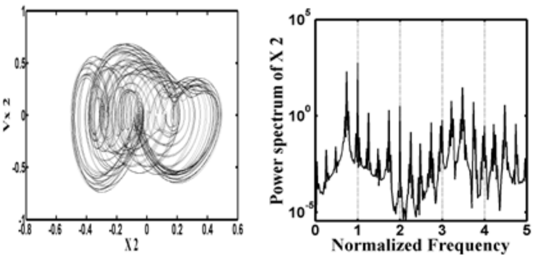

3.2(a) 3.2(b)

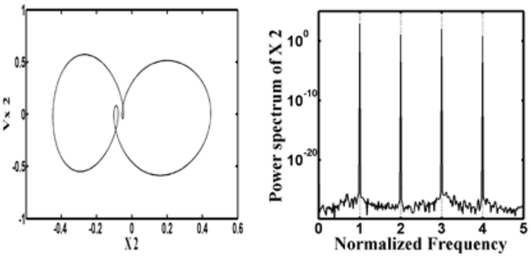

3.3(a) 3.3(b)

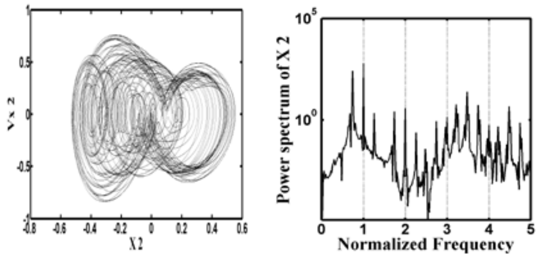

3.4(a) 3.4(b)

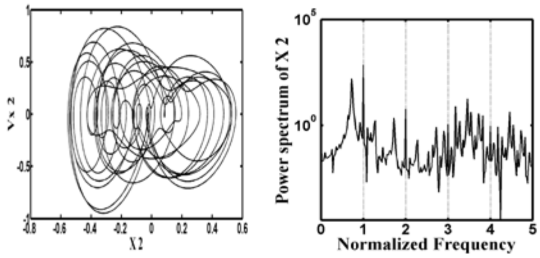

3.5(a) 3.5(b)

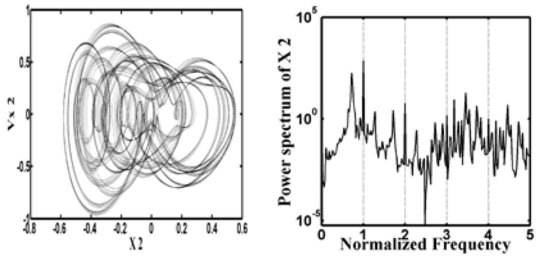

3.6(a) 3.6(b)

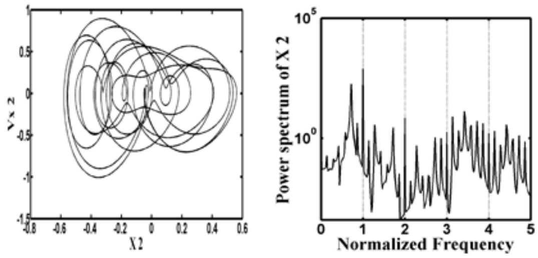

3.7(a) 3.7(b)

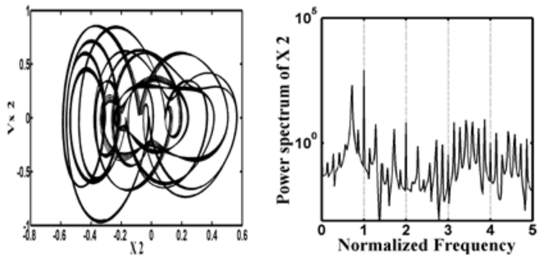

3.8(a) 3.8(b)

Fig. 3. The rotor center phase diagram of the small hole-shallow chamber throttle air pressure bearing system when the rotor mass m_r = 3.2, 4.54, 4.85, 4.91, 5.43, 5.48, 5.85, 5.93 kg (Fig. 3.1a-3.8a)), and the spectral response diagram of the rotor center in the horizontal direction (Fig. 3.1b-3.8b) with Λ=3.8.

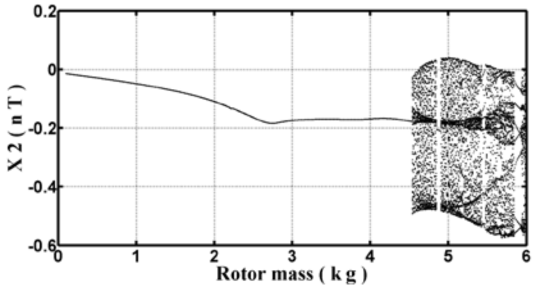

4(a)

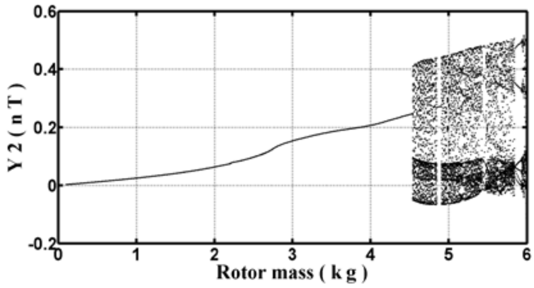

4(b)

Fig. 4. Bifurcation diagram of the rotor center of the small hole-shallow chamber throttle air pressure bearing system to different rotor masses (a) X2(nT) (b) Y2(nT), with Λ=3.8.

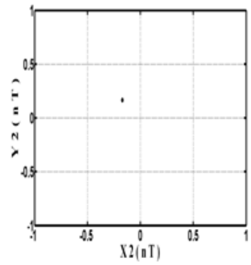

5(a)

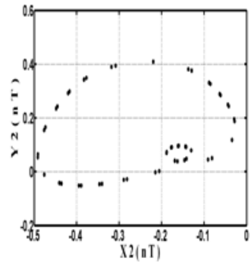

5(b)

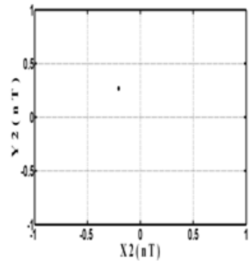

5(c)

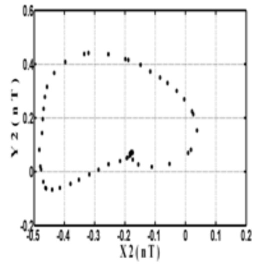

5(d)

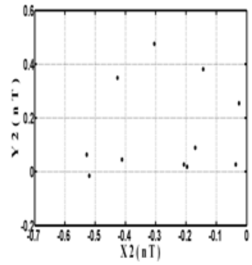

5(e)

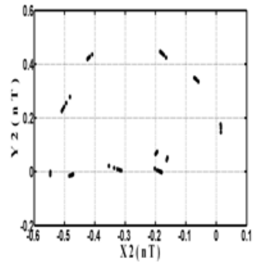

5(f)

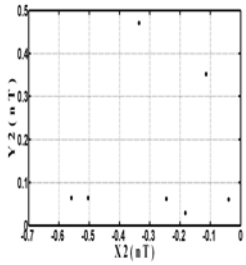

5(g)

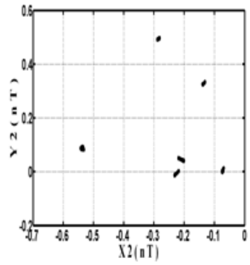

5(h)

Fig. 5. Poincaré maps of the rotor center of the small hole-shallow chamber throttle air pressure bearing system at different rotor masses (a) m_r = 3.2,, (b)4.54, (c)4.85, (d)4.91, (e)5.43, (f)5.48, (g)5.85, (h)5.93 kg

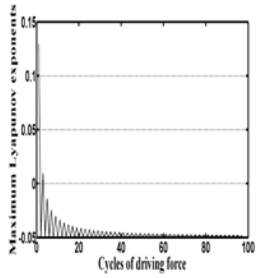

6(a)

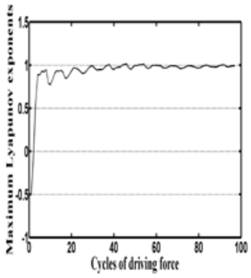

6(b)

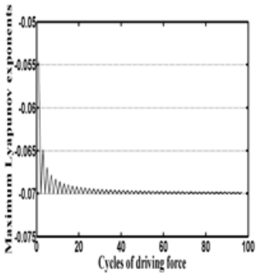

6(c)

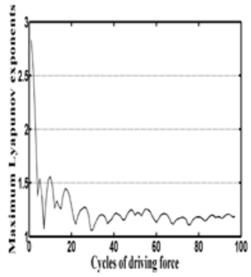

6(d)

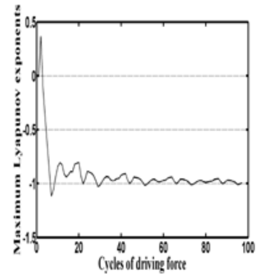

6(e)

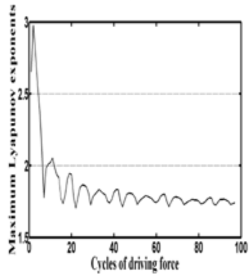

6(f)

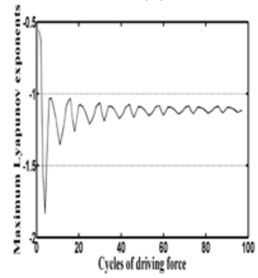

6(g)

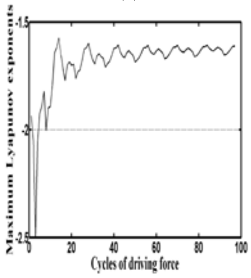

6(h)

Fig. 6. The maximum Lyapunov exponents of the rotor center of the small hole-shallow chamber throttle air pressure bearing system at different rotor masses (a) m_r = 3.2,, (b)4.54, (c)4.85, (d)4.91, (e) 5.43, (f) 5.48, (g) 5.85, (h) 5.93 kg.

Dynamic behavior analysis – bearing number as a bifurcation parameter

Take the annular throttle air bearing system as an example. For this bearing system, the bearing number (rotation speed) directly affects the pressure distribution in the bearing, as well as the relative performance and stability of the entire system. Therefore, in this section, the bearing number (Λ) is used as the bifurcation parameter, and the rotor mass is set as m_r=3.47 kg. The relevant dynamic behavior of the bearing system is analyzed and discussed:

From Fig. 7.1(a), 7.2(a), .., 7.9(a), it can be seen that when the bearing number is small (Λ=1.0, 1.2), the rotor behavior presented irregular motion, and when Λ increases to 1.91 and 4.5, regular movement appears. Meanwhile, the behavior of the rotor center turns into a regular and symmetrical phenomenon. When Λ continues to increase to 9.03, 9.38, 14.3, the dynamic trajectory maintains a relatively regular periodic motion, and at Λ=16.41, irregular motion appears again. When Λ increases to 18.2, the rotor center becomes regular behavior. From the above results, it can be ascertained that the change in the bearing number does have significantly effects on the system, and the behavior of rotor is caused by the slight change of bearing number and performed the aperiodic and periodic motions. It can be seen that Λ is the sensitive and important factor to the bearing system.

Figure 7.1(b), 7.2(b),..., 7.9(b) shows the frequency spectrum response of the rotor center in the horizontal direction when the bearing number is different. As Λ=1.0 and 1.2, the rotor center exhibits non-periodic motion, and when Λ=1.91 and 4.5, the spectral response shows that the rotor center has a T periodic motion. While Λ=9.03, the system is sub-periodic motion; and when Λ=9.38 and 14.3, the motion mode is changed to T-period motion. When Λ=16.41, the non-periodic motion reappears, until Λ=18.2, the system is stable again.

The bearing number Λ is used as the main analysis parameter to discuss the influence of different bearing number Λ on the air bearing system as shown in Fig. 8. At the same time, the bearing number range is set between 1.0 and 19.0 for actual operating conditions. When bearing number is low as Λ=1.0 and 1.2, the rotor center of the system exhibits aperiodic chaotic motion in both the horizontal and vertical directions. This phenomenon can be verified by the Poincaré maps in Fig. 9(a) and (b). It is known that there are multiple discrete points on the Poincaré maps, and this type of motion occurs in the interval 1.0≦Λ<1.91. When the bearing number increases to Λ=1.91, the system bifurcates and produces T-periodic motion. It can be clearly seen from Fig. 9(c) that the system produces a discrete point at this time, and this T-periodic motion continues in 1.91≦Λ<9.03 interval (where Λ=4.5, the system also moves in T-period, as shown in Fig. 9(d)). When the bearing number increases to the interval of 9.03≦Λ<9.38, the system turns to 4T periodic motions. As shown in Fig. 9(e), it can be verified that there are 4 discrete points. When Λ=9.38, this state of motion will change to T-period motion, as shown in Fig. 9(f). This behavior occurs in the interval 9.38≦Λ<16.41 (where Λ=14.3, the system is also in T-period motion, such as Fig. 9(g) shows). In the interval of 16.41≦Λ<18.2, the system once again produces chaotic motion, as shown in Fig. 9(h). However, when this unstable state is further changed to Λ=18.2, the system becomes stable and exhibits T periodic motion, and this behavior continues to be Λ=19.0, as shown in Fig. 9(i).

As to whether the chaotic behavior is caused by the change of the bearing number, the maximum Lyapunov exponents are also used to verify as shown in Fig. 10(a), 10(b) and 10(h). It can be seen that when Λ = 1.0, 1.2, 16.41, the index is all greater than zero meaning that the motion state of the system is chaotic behavior. Conversely, from Fig. 10(c), 10(d), 10(e), 10(f), 10(g), 10(i), we can see that the index is equal to or less than zero when Λ=1.91, 4.5, 9.03, 9.38, 14.3 and 18.2, so the non-chaotic behavior of the system is consistent with the above results.

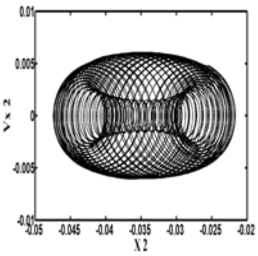

7.1(a)

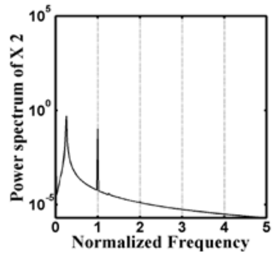

7.1(b)

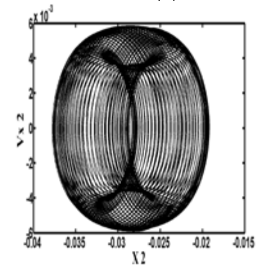

7.2(a)

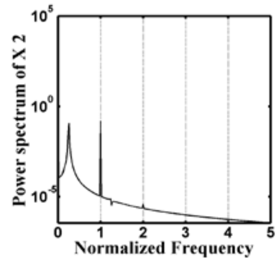

7.2(b)

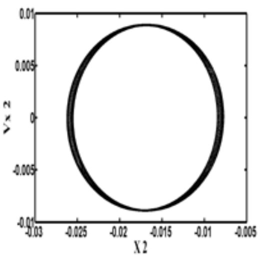

7.3(a)

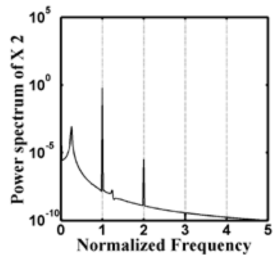

7.3(b)

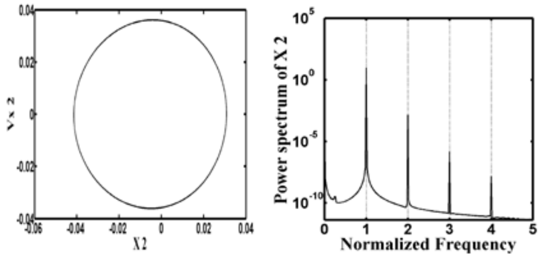

7.4(a) 7.4(b)

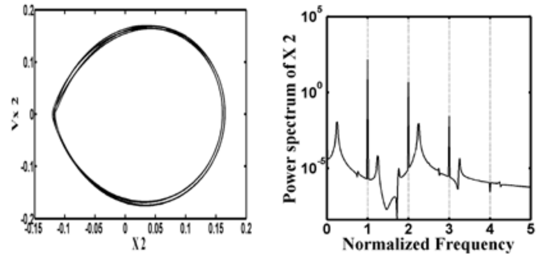

7.5(a) 7.5(b)

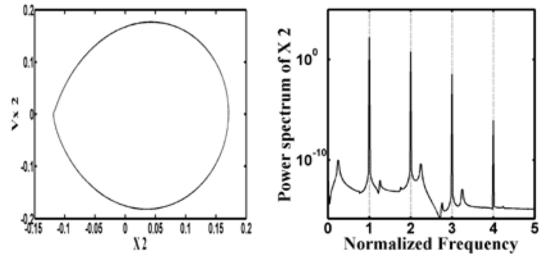

7.6(a) 7.6(b)

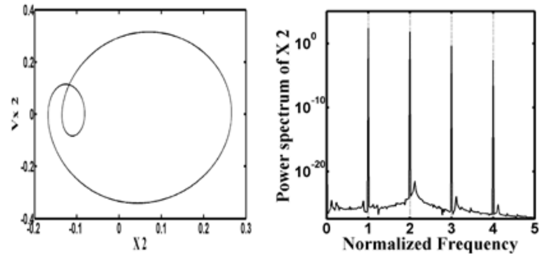

7.7(a) 7.7(b)

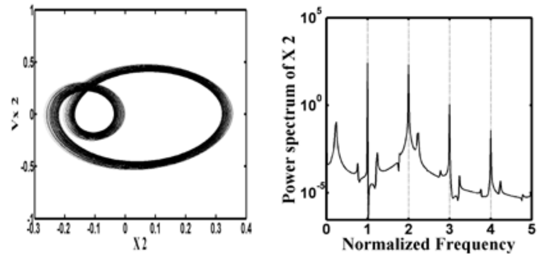

7.8(a) 7.8(b)

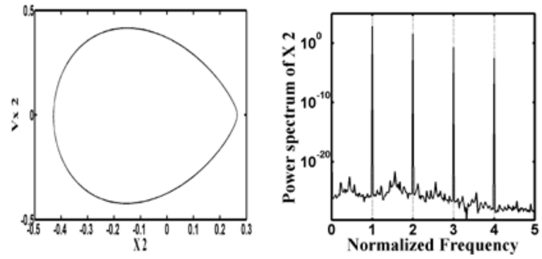

7.9(a) 7.9(b)

Fig. 7. The phase diagram of the rotor center of the annular throttle air bearing at Λ = 1.0, 1.2, 1.91, 4.5, 9.03, 9.38, 14.3, 16.41, 18.2 (Fig. 7.1a-7.9a), and the frequency spectrum response of the rotor center in the horizontal direction (Fig. 7.1b-7.9b) with rotor mass m_r=3.47kg.

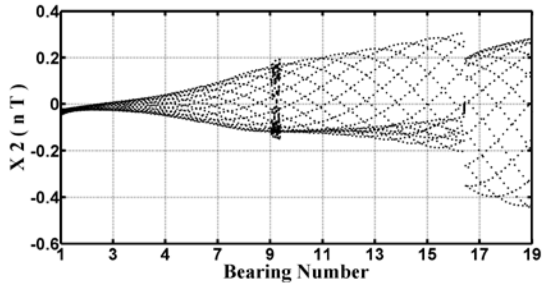

8(a)

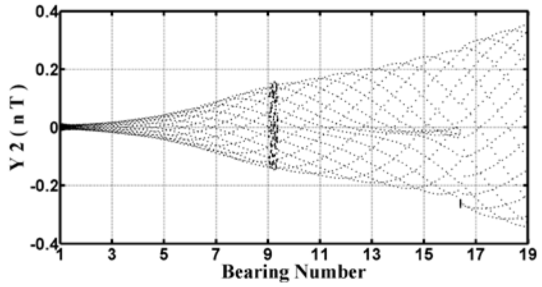

8(b)

Fig. 8. Bifurcation diagram of the rotor center to different bearing numbers Λ of the annular throttle air bearing system: (a) X2(nT) (b) Y2(nT), the rotor mass m_r = 3.47 kg.

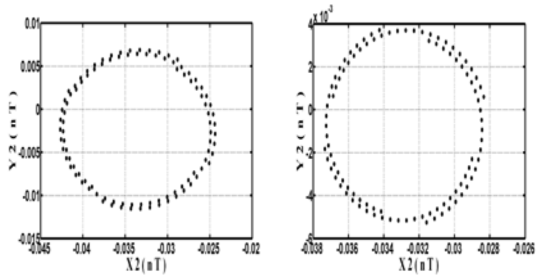

9(a) 9(b)

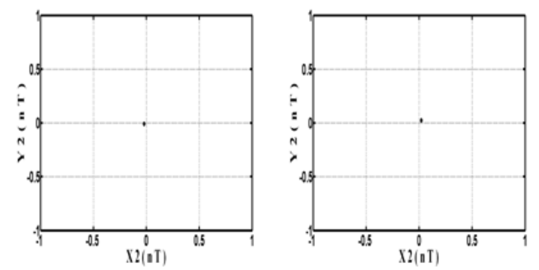

9(c) 9(d)

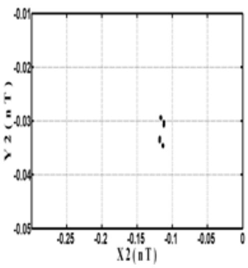
9(e)

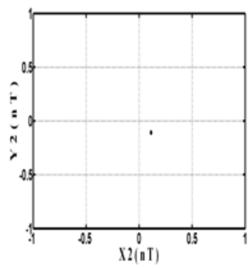
9(f)

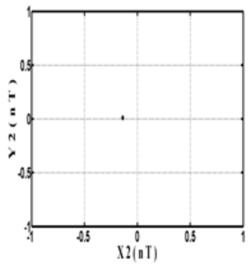
9(g)

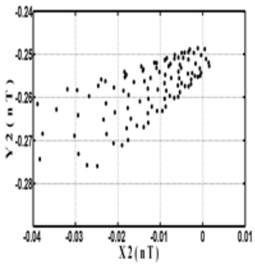
9(h)

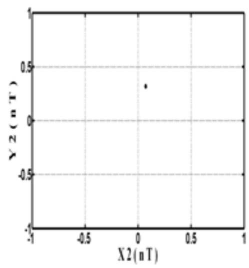
9(i)

Fig. 9. Poincaré maps of the rotor center of the annular throttle air bearing system with different bearing numbers Λ = (a) 1.0, (b)1.2, (c)1.91, (d)4.5, (e)9.03, (f)9.38, (g)14.3, (h)16.41, (i)18.2.

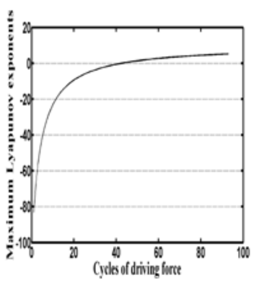
10(a)

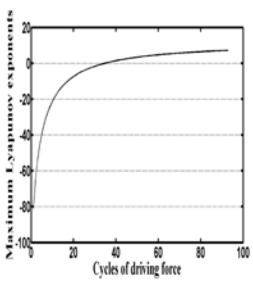
10(b)

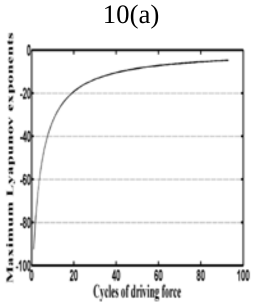
10(c)

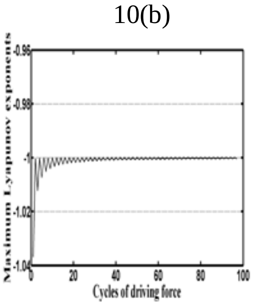
10(d)

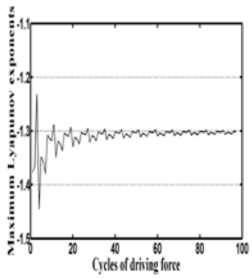
10(e)

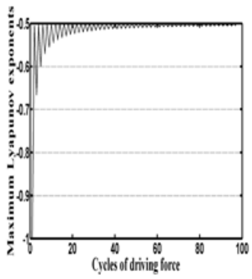
10(f)

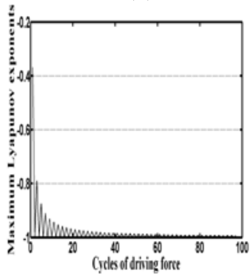
10(g)

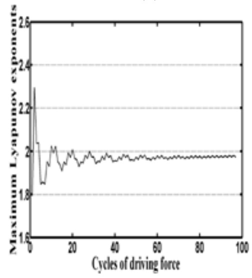
10(h)

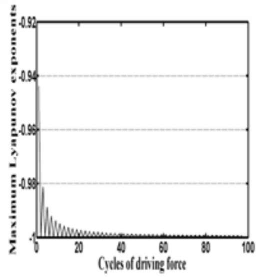
10(i)

Fig. 10. Maximum Lyapunov exponent of the rotor center of the annular throttle air bearing system at different bearing numbers Λ= (a) 1.0, (b)1.2, (c)1.91, (d)4.5, (e)9.03, (f) 9.38, (g)14.3, (h)16.41, (i)18.2.

CONCLUSIONS

The objective of this study was an analysis of the dynamic behaviour of a pocket-orifice compensated air bearing (PCAB) system. The design of the orifice is divided into two types including small hole-shallow chamber throttle type and annular throttle type. The flexible rotor supported by a pocket-orifice compensated air bearing system is analyzed. The perturbation method and a hybrid method were used to solve the pressure distribution at the highest nonlinearity in the system, after which dynamic equations of the flexible rotor center were used to obtain the orbits displacement. Analysis was then conducted on the orbit data to generate spectrum diagrams, Poincaré maps, bifurcation diagrams and maximum Lyapunov exponents. The simulation results showed that the hybrid method applied in this paper yields better accuracy and precision for the verification of values than perturbation method. Accurate solutions can be obtained without the need for using small mesh size and time step determination. The dynamic results of rotor center reveals that the rotor behavior changes along with the rotor mass and the bearing number and synchronously generate complicated motion in the horizontal and vertical directions, include periodic and sub-harmonic vibration, as well as quasi-periodic and chaotic motions. Especially for the chaotic motion, this unstable can be detected efficiently by our proposed method and contributed to provide the chaotic intervals for various parameters of rotor mass and bearing number. The results obtained in this study can be used as a basis for future PCAB system design and the prevention of instability.

ACKNOWLEDGMENT

Financial support for this work was provided by the Ministry of Science and Technology, Taiwan, under the contract MOST 108-2221-E-167 -028**.**

REFERENCES

Bently, D., "Forced Subrotative Speed Dynamic Action of Rotating Machinery," *ASME Paper No. 74-PET-16*, *Petroleum Mechanical Engineering Conference, Dallas. Texas*, (1974).

Charki, A., Diop, K., Champmartin, S. and Ambari. A., "Numerical Simulation and Experimental Study of Thrust Air Bearings with Multiple Orifices," *Int. J. Mech. Sci.*, Vol. 72, pp.28-38 (2013).

Childs, D.W., "Fractional-Frequency Rotor Motion Due to Nonsymmetric Clearance Effects," *ASME J. Eng. Gas. Turbines Power*, Vol. 104, pp. 533-541 (1982).

DeGast, J.G.C., "A New Type of Controlled Restrictor (M.D.R.) for Double Film Hydrostatic Bearings and Its Application to High-Precision Machine Tools," *Proceedings of the 7th international M.T.D.R. conference, Birmingham*, pp.273–298 (1966).

Ghosh, B., "Load and Flow Characteristics of a Capillary-Compensated Hydrostatic Journal Bearing," *Wear*, Vol. 23, pp. 377-386 (1973).

Malanoski, S.B. and Loeb, A.M., "The Effect of the Method of Compensation on Hydrostatic Bearing Stiffness," *J. Basic Eng.*, Vol. 83, No. 2, pp. 179-185 (1961).

Mayer, J.E. and Jr. Shaw, M.C., "Characteristics of an Externally Pressurized Bearing Having Variable External Flow Restrictors," *J. Basic Eng.*, 1963, Vol. 85, No. 2, pp. 291-296 (1963).

Reynolds, O., "On the Theory of Lubrication and Its Application to Mr. Beauchamp Tower's Experiments, Including an Experimental Determination of the Viscosity of Olive Oil," *Philos Trans. R. Soc. London, Ser A*, Vol. 177, pp.157–234 (1886).

Robert, S., "Regulator for Adjusting the Fluid Flow in a Hydrostatic or Aerostatic Device," *Appl. No. EP1007861. European Patent Office.* (2002).

Rowe, W.B. and O'Donoghue, J.P., "Diaphragm Valves for Controlling Opposed Pad Bearings," *Proc. Inst. Mech. Eng*., Vol. 184, pp. 1-9 (1969).

Wang, C.C., "Non-Periodic and Chaotic Response of Three-Multilobe Air Bearing System," *Appl. Math Modell.* Vol. 47, pp. 859-871 (2017).

Wang, C.C. and Lee, T.E., "Nonlinear Dynamic Analysis of Bi-Directional Porous Aero-Thrust Bearing Systems," *Adv. Mech. Eng.* Vol. 9, No. 12, pp. 1-11 (2017).

Wang, C.C., Lee, R.M., Yau, H.T. and Lee, T.E., "Nonlinear Analysis and Simulation of Active Hybrid Aerodynamic and Aerostatic Bearing System," *J. Low Freq. Noise Vibr. Act. Control*, Vol. 38, No. 3-4, pp. 1404-1421 (2019).

腔孔節流氣壓軸承系統之動態分析研究

汪正祺
國立勤益科技大學
張致文
國立聯合大學
李素娥
亞洲大學

摘 要

本文旨在探討腔孔節流氣壓軸承系統針對高轉速、高剛性、高精度支承需求之精密儀器與機構的氣膜潤滑問題。此軸承由於具有外部供氣及腔孔節流兩種特性與優點，因此可提供較其他氣膜軸承系統具有更優異的穩定性。研究此軸承系統時，由於氣膜壓力函數具有強烈的非線性，且實際軸承系統所具有的動態問題包含臨界速度、供氣失衡或軸承設計不當等，都將導致轉子軸承系統在某些參數條件下，其旋轉過程中產生非週期或混沌運動及不穩定的現象。而這些不規則運動嚴重時甚至造成機件損傷或破壞，因此為能瞭解系統在工作的過程中何種狀況下會產生非週期的現象，以避免產生不規則的振動效應，本文以微擾法及混合法等數值分析的方式將軸承的相關特性做一詳盡的探討，並以相關理論包括分岔圖、龐卡萊映射、頻譜響應及李奧維指數針對轉子之非線性行為進行研究分析。結果顯示，以軸承數Λ為例，軸承數會影響轉子的軌跡與軸承系統性能，尤其轉子的動態軌跡在 16.41≤Λ<18.2 的區間內會產生非線性混沌行為，此種非週期性行為會造成軸系損害。本研究所獲得的結果可以用作將來腔孔節流氣壓軸承系統的穩定性設計和防止轉子產生動態不穩定的設計基礎及重要依據。